

HYDROGEN AND CARBON SPECIATION IN NOMINALLY ANHYDROUS MINERALS OF LITHOSPHERIC MANTLE ROCKS: A COMPREHENSIVE FTIR AND STA + QMS STUDY

© 2020 M. S. Babushkina^{1,*}, L. P. Nikitina¹, A. G. Goncharov^{1,2}, and V. L. Ugolkov³

¹*Institute of Precambrian Geology and Geochronology RAS,
Makarova nab., 2, Saint-Petersburg, 199034 Russia*

²*Saint-Petersburg State University, Institute of Earth Sciences,
Universitetskaya nab., 7/9, Saint-Petersburg, 199034 Russia*

³*Institute of Silicate Chemistry RAS, Makarova nab., 2, Saint-Petersburg, 199034 Russia*

*e-mail: msbab@mail.ru

Received July 4, 2019; Revised October 30, 2019; Accepted November 6, 2019

The presence of hydrogen and carbon in forms of OH⁻ ions, molecules of crystal hydrate water (H₂O_{cryst}) and specific groups CO₂, CH, CH₂, CH₃ has been found in crystal structures of mantle minerals by Fourier-Transform Infrared Microspectroscopy (FTIR) and Simultaneous Thermal Analysis in combination with Quadrupole Mass Spectrometry of thermal decomposition products (STA + QMS) methods. Temperature of m17 (OH⁻) release is higher (STA + QMS data) in comparison with m18 (H₂O), that testify to weaker bonds of H₂O_{cryst} in the crystal structure which is supported by higher values of wavenumbers of ν_{OH⁻} compared to ν_{H₂O_{cryst}}. The water component (OH⁻ + H₂O_{cryst}) is predominant among volatiles. It is equal (ppm): 40–400 in diopside, 20–220 in enstatite, 10–230 in forsterite, and 30–340 in pyrope, with up to 200 ppm bulk content in xenoliths. The volatiles preserve in the NAMs structure at widely range temperature (750–1450 °C), pressure (1.5–5.5 GPa), and the oxygen fugacity [Δ log fO₂^{FMQ} (−4.5...+0.3)]. The main mechanism of its release from the minerals is, probably, partial melting process: the total content of water component decreases with increasing degree of partial melting.

Keywords: hydrogen, carbon, FTIR, STA + QMS, lithospheric mantle xenolith, peridotite, pyroxenite, nominally anhydrous minerals

DOI: 10.31857/S0869605520010050

INTRODUCTION

Contents, forms, and storage conditions of volatile components, such as hydrogen and carbon species, in the crystal structure of rock-forming minerals of upper mantle peridotites and pyroxenites are of great importance in understanding the properties of the lithospheric mantle: melting relations, phase assemblages, rheology, seismic properties, and electrical conductivity of upper mantle rocks. Previous FTIR and SIMS studies have shown that mantle nominally anhydrous minerals (NAMs) contain hydrogen and carbon as structurally bound volatiles incorporated in crystal structures. The water content in NAMs varies widely: from a few to 300 ppm in olivine (*ol*), from 60 to 650 ppm in orthopyroxene (*opx*), from 1 to 160 ppm in garnet (*grt*), and from 100 to 1300 ppm in clinopyroxene (*cpx*) (Bell, Rossman, 1992a, b; Kadik, 2006; Grant et al., 2007; Yang et al., 2008; Babushkina et al., 2009; Doucet et al., 2014; Goncharov et al.,

2015; Demouchy, Bolfan-Casanova, 2016). Up to ten times variation in water content in these minerals may be a consequence of various reasons, such as their chemical composition and conditions of crystallisation and alteration. Despite relatively low contents of structurally bound hydroxyl (tens to few hundred ppm) in forsterite, enstatite, or diopside, which compose major portion of the lithospheric mantle, it can be reasonably assumed that these phases are a potential storage of the water in the mantle.

Experiments performed over a wide range of conditions, show significant dependence of water solubility in mantle minerals on temperature and notably on pressure for olivine (Bai, Kohlstedt, 1992; Withers, Hirschmann, 2008; Litasov et al., 2009; Ardia et al., 2012; Yang, 2015), orthopyroxene (Rauch, Keppler, 2002), clinopyroxene and garnet (Geiger et al., 1991), perovskites and periclase (Murakami et al., 2002). Experimental data also indicate the influence of O₂ and H₂O fugacity on water solubility in the crystal lattice (Kadik, 2006; Bali et al., 2008; Férot, Bolfan-Casanova, 2012). The aspects of hydrogen crystal chemistry in the NAMs crystal structure are reviewed earlier (Smyth et al., 1997, 2007; Matsyuk et al., 1998; Kohn et al., 2002; Matsyuk, Langer, 2004; Koch-Müller et al., 2004, 2006, 2007; Jacobsen et al., 2005; Mosenfelder et al., 2006; Freund, Freund, 2006, 2015; Berry et al., 2007; Gavrilenko, 2008; Mosenfelder, Rossman, 2013a; b; Balan et al., 2014).

Results of numerous studies of the proton position in the crystal structures of mantle minerals, due to the low content do not allow a creation of the reliable models of its localization. There are different substitution mechanisms for the OH⁻ incorporation in the olivine structure, namely OH⁻ associated with Si⁴⁺ vacancies in tetrahedron or cation (Mg²⁺, Fe²⁺, Fe³⁺) vacancies in M1, M2 octahedron and also may be present in the interstices (Kohlstedt et al., 1996; Karato, 2006). The number of publications (Khisina et al., 2001, 2008; Khisina, Wirth, 2002) describe nanoinclusions in *ol* from peridotite xenoliths in the kimberlite pipe "Udachnaya", Siberian craton. The inclusions containing OH⁻ have (Mg + Fe)/Si ratio less than host *ol* and is described with the formula (Mg_{1-x}Fe_y²⁺)_{2-x}V_xSiO₄H_{2x}, where V are vacancies in cation sublattice, presuming they are decomposition products of the primary *ol* saturated with OH⁻ point defects.

Pyroxene and garnet are multicomponent solid solutions. The presence of water in these minerals is more complicated compared to olivine. Different associations of hydrogen with cations (Al, Ca, REE) both in octahedral and tetrahedral crystallographic positions take place in their crystal structure (Smyth et al., 1997, 2007). In *cpx* which has the most complex and multi-component structure, proton has the potential possibility to occupy a different structural locations. The change in the content of Al or other trivalent cations increases the probability of hydrogen entry in the pyroxene structure (Rauch, Keppler, 2002; Stalder, 2004; Mierdel et al., 2007; Stalder, Ludwig, 2007; Gavrilenko, 2008; Férot, Bolfan-Casanova, 2012).

The solubility of carbon in mantle minerals is much less compared to hydrogen. Carbon contents in enstatite, diopside, and pyrope grown from carbonatite melts enriched with isotope ¹³C at 900–1400 °C and 1.5–16 GPa are in the range of 0.1–1 ppm (Shcheka et al., 2006). The carbon content in olivine is increased by two orders of magnitude at the change of pressure from 1 to 11 GPa with the maximum content about 12 ppm (Shcheka et al., 2006). Data on the solubility of C in olivine were published in (Freund, 1981; Freund et al., 1986; Tingle, Green II, 1987; Tingle et al., 1988), although they were not confirmed altogether (Mathez et al., 1984; Tsong et al., 1985; Tsong, Knipping, 1986). The probability of carbon presence in the crystal lattice of olivine was considered as negligible (Mathez et al., 1984). High concentration of C (425 ppm) in one olivine sample is presumably explained by a presence of discrete C-enriched phases in the form of submicroscopic inclusions. The carbon content in spinel is below the detection limit (30 ppb). For minerals of mantle transition zone (wadsleyite, ringwoodite, MgSiO₃-ilmenite, MgSiO₃-perovskite) carbon contents are also below the limit of detection (40–110 ppb). And there are no clear dependencies of carbon solu-

bility on temperature, oxygen fugacity, and the iron content (Shcheka et al., 2006). Carbon (as a part of groups with C–H and C–O bonds), as well as water, may be associated in crystals structures of mantle minerals with cation vacancies in tetrahedron and octahedron positions or interstices (Freund, 1981; Freund et al., 1986; Freund, Freund, 2006), and as C⁴⁺, substituting Si⁴⁺ (Shcheka et al., 2006).

Most of the published data on water and carbon presence in the NAMs crystal structure has been obtained by Fourier-Transform Infrared (FTIR) Spectroscopy. The method, among the others (SIMS, ERDA, 1H MAS NMR), is the most sensitive for determination of structure-related volatiles, non-destructive and has the highest analytical accuracy. However, the question of the forms and content of hydrogen and carbon in mantle minerals, conditions of their storage in the upper mantle is still studied insufficiently and requires confirmation by other methods, for example, such as Simultaneous Thermal Analysis in combination with Quadrupole Mass Spectrometry of thermal decomposition products (STA + QMS). These methods allow simultaneous investigation of changes in mass, enthalpy, and decomposition products using mass spectrometric studies of released gases.

The aims of the present work are: (1) the study of mantle rock-forming minerals (diopside, forsterite) by FTIR and STA + QMS methods for reasonable conclusions about presence of various forms of hydrogen (OH⁻ and H₂O) and carbon (C–O and C–H bonds) species in their crystal structures; (2) the study of releasing temperatures of various hydrogen and carbon species in the structure of forsterite and diopside by STA + QMS method; (3) the determination of volatile contents in minerals of mantle xenoliths from basalts and kimberlites of several regions by FTIR; (4) the study of behaviour of volatiles depending on crystallization conditions of mineral assemblages in mantle xenoliths.

EXPERIMENTAL METHODS

Fourier-transform infrared (FTIR) spectroscopy. Analyses have been performed using single crystals of minerals prepared in a form of plane-parallel plates, double-faced polished, with a diameter changed from 1.0 to 3.0 mm and thickness of 150–400 µm, measured with the accuracy of ±2 µm (Babushkina et al., 2009; Goncharov et al., 2015). Plates were polished with fine (1.0 µm) diamond paste. After that they were washed in baths, first with acetone and then with alcohol. Homogeneity of grains and absence of gas-liquid and solid inclusions were checked with the optical microscope examination (LOMO Polam R211). Infrared spectra were obtained with Vertex 70 Fourier spectrometer equipped with IR Hyperion 1000 microscope (Saint Petersburg Mining University, Saint Petersburg), from 400 to 7500 cm⁻¹ with the resolution of 4 cm⁻¹, by accumulating 32 scans and with a squared aperture, with 20 or 100 µm of wideness. Spectra were fitting using Peak Fit (v. 4.12) program with specified form lines of “Voigt area G/L” and linear form of the baseline ($R^2 \approx 0.98\text{--}0.99$ for the fittings). All spectral parameters were varied.

The analyses were performed using unpolarized infrared light in optical pure areas of mineral plates free of gas-liquid inclusions and cracks and available for clear path through the minerals. Background spectra were recorded before each measurement. For some samples, spectra were obtained earlier (Babushkina et al., 2009) with the IFS88 BRUKER Fourier spectrometer equipped with IR microscope (Institute of Macromolecular Compound RAS, Saint Petersburg). The recording was performed with a constant purge of the sample cell with dry air, H₂O- and CO₂-free, to avoid absorption of atmospheric water and carbon dioxide. Both studies showed identical results. For all samples spectra were recorded for some mineral grains (from 2 up to 4) and for each grain in several points. The possibility of using unpolarized IR light to determine the concentrations of structural hydroxyl accurately even from few ($n > 5$) unoriented anisotropic grains of minerals is justified in the works of Kovács et al. (2008) and Sambridge et al. (2008). The accuracy of pyroxene measurements can be still satisfactory if less

than 5 or even only one unoriented grains are considered (Xia et al., 2013; Liu et al., 2015). It is clear that the greater of unoriented grains investigated, the more accurate is the assessment, but obtaining a large number of high-quality mineral grains from xenolith is very difficult. The spread of values of water content was near 10–15% that has allowed to average the results. The results, obtained for a few grains of the same mineral, have given comparable values of water content at different points of the grain, that testifies to the validity of the obtained data.

A thorough examination of FTIR spectra of minerals was made in absorption regions of stretching vibrations (ν) of OH⁻ (3750–3450 cm⁻¹), stretching (3450–3000 cm⁻¹) and deformation (δ , 1680–1530 cm⁻¹) vibrations of crystal hydrate water molecules H₂O_{cryst}, and stretching vibrations of characteristic groups with C–H (2900–2850 cm⁻¹) and C–O (2350 cm⁻¹) bonds. Absorption in the IR spectrum of minerals in regions 3450–3000 and 1680–1530 cm⁻¹ is an important evidence of the presence of crystal hydrate water molecules that have not lost their chemical individuality and form relatively weak hydrogen bonds in the structure of a mineral (Lazarev, 1995). The content of water (ppm) was calculated from integral intensities of absorption bands of stretching vibrations of OH⁻ and H₂O_{cryst} normalized to a thickness of 1 cm. The calculations were made for the entire spectrum region 3750–3000 cm⁻¹ without division into OH⁻ and H₂O_{cryst} using the calibrations for pyroxene, olivine, and garnet given by Bell et al. (1995, 2004).

Molar extinction coefficients for various carbon molecules in the structure of NAMs, which allow determining contents of these groups on the basis of integral intensities of absorption bands of stretching vibrations of CH (2850–2900 cm⁻¹) and CO (2350 cm⁻¹), are not determined yet. In this connection, only ratios of parts of water (A_{H₂O}^{tot}) and characteristic carbon groups (A_{CH}, A_{CO}) have been determined from the ratio of integral intensities I of absorption bands of stretching vibrations of bonds of OH⁻, H₂O_{cryst} and groups CH, CO, divided by the thickness of the plate, according to equations:

$$\begin{aligned} A_{CH} &= \frac{I_{CH}}{I_{CO} + I_{CH} + I_{H_2O}}, & A_{CO} &= \frac{I_{CO}}{I_{CO} + I_{CH} + I_{H_2O}}, \\ A_{H_2O} &= \frac{I_{H_2O}}{I_{CO} + I_{CH} + I_{H_2O}}, \end{aligned} \quad (1)$$

where I is integral intensity of the absorption bands of required component, $I_{H_2O} = I_{OH^-} + I_{H_2O_{cryst}}$, $I_{CH} = I_{CH_2} + I_{CH_3}$, $I_{CO} = I_{CO_2}$. These formulas allow us to make a semi-quantitative assessment of the volatile ratio in the crystal structure.

The simultaneous thermal analysis in combination with quadrupole mass spectrometry of thermal decomposition products (STA + QMS). The analyses have been performed using the same plates for which ratio of volatiles was identified previously according to FTIR spectra. It was proposed to determine which gases are released from minerals during heating in the temperature range of equipment 40–1300 °C. Complex thermal analysis was performed in the Institute of Silicate Chemistry RAS on STA 429 CD NETZSCH equipment using sample holder of “DSC + TG” type with platinum-rhodium (10%) thermocouples in platinum-rhodium crucibles. Before conducting thermal studies samples have been weighed with analytical balance with the accuracy of ±0.01 mg, placed in the crucible and set into a furnace. Before carrying out analysis internal space of the furnace has been pumped to residual pressure about 2×10^{-4} bar and then high pure argon has been filled and analysis has been performed in this stream during all heating from 40 to 1300 °C at rate 20 °C per minute. Value of argon flow rate was (40 ± 10) ml per minute. Qualitative and quantitative mass spectrometry composition was determined in the flow of gases going from the furnace with the help of quadrupole QMS 403 C mass spectrometer of the German company NETZSCH connected by heated quartz capillary with STA 429

CD. Thus heating was accompanied with simultaneously recording changes in mass of the sample – TG curve, changes in internal energy or enthalpy – DSC curve, and changes in the content of different masses in decomposition products – curves IC (ion current), corresponding to various values of m/z numbers. The empty crucibles were investigated before thermal studies and after them to obtain a course of “zero lines” in conditions that fully complies with conditions of further tests, that allowed to get in the following more correct results. The samples have been photographed with a microscope MPB-2, with 24 \times magnification before study and after reaching temperature of 1300 °C. The studies carried out in the temperature range of 40–1300 °C have allowed obtaining information about changes in the mass of the samples of forsterite and diopside, internal energy or enthalpy, and change of IC, corresponding to various values of m/z numbers.

Ratios of parts of water ($A_{H_2O}^{tot}$) and characteristic carbon groups (A_{CH} , A_{CO}) have been determined similarly to FTIR from the ratio of ion current values of peaks of releasing of OH⁻, H₂O_{cryst} and groups CH, CO, normalized to the mass of the plate at different temperatures, according to equations (1), where I for STA + QMS data is value of IC of the corresponding temperature peak of releasing of m17, m18, m12, m13, m14, m15, m16 and m44.

RESULTS

Forsterite and diopside investigation with FTIR and STA + QMS. A comprehensive analyses have been performed for optical pure plates of three samples of forsterite (IA2, IA675, IA388) and one sample of diopside 878-01 from xenoliths of mantle spinel and garnet peridotites. FTIR spectra are shown in Figs. 1–3. Spectra of diopside and forsterite show absorption bands of stretching vibrations of hydroxyl ion (diopside: 3652, 3618, 3575, 3524, and 3460 cm⁻¹, and forsterite: 3639, 3597, 3571, 3554, 3521, and 3478 cm⁻¹) and molecules of crystal hydrate water (diopside: 3409, 3345 cm⁻¹ and forsterite: 3403 cm⁻¹). The number and positions of bands in the spectra of minerals are determined by compositions and by the number of possible combinations of cations in the nearest cation coordination sphere. Spectra of these minerals also show characteristic absorption bands of symmetrical (v^s) and antisymmetric (v^{as}) stretching vibrations of C–H bonds in the carbon groups CH₂ and CH₃ (Fig. 2a, b). Stretching bands of carbon groups with C–O bonds 2356, 2347, and 2340 cm⁻¹ are observed in the spectrum of diopside (Fig. 3, a). The spectrum of forsterite shows absorption peaks 2360, 2351, 2341, 2332 cm⁻¹ in this region (Fig. 3, b). The positions of absorption bands (cm⁻¹) with the correlation to the valence vibrations in hydrogen and carbon groups in the forsterite and diopside spectra are presented in (Babushkina et al., 2018).

Thermograms of forsterite and diopside in temperature range from 40 to 1300 °C (Fig. 4) show peaks of release of groups with masses m17, m18, assigned with OH⁻, H₂O, accordingly. Peaks of release of m17 are observed in forsterite at 839, 858 and 1255, 1285 °C (Fig. 4, a) and ones of m18 at 694 and 1194 °C (Fig. 4, b). Forsterite characterized by the excess of IC of m18 by three orders of magnitude in relative to m17. This result is in agreement with FTIR data that H₂O_{cryst} prevails over OH⁻ in forsterite. Changes of m17 (OH⁻) and m18 (H₂O) in diopside are smooth in the range of 400–1300 °C and IC of m17 exceed slightly IC of m18. The course of enthalpy change curves shows that starting from 950 °C, exothermic effects, similar in form but different in size, associated probably with different processes (oxidation, destruction, and release of volatiles) are observed for all four samples. The release of m17 (OH⁻) occurs at the higher temperature than one of m18 (H₂O), that testify to weak bonds of crystal hydrate water with minerals structure in comparison with hydroxyl ions. The presence of several peaks of releasing for m17 and m18 may testify to different cation environment in the nearest coordination sphere of hydroxyl ion and molecules of crystal hydrate water.

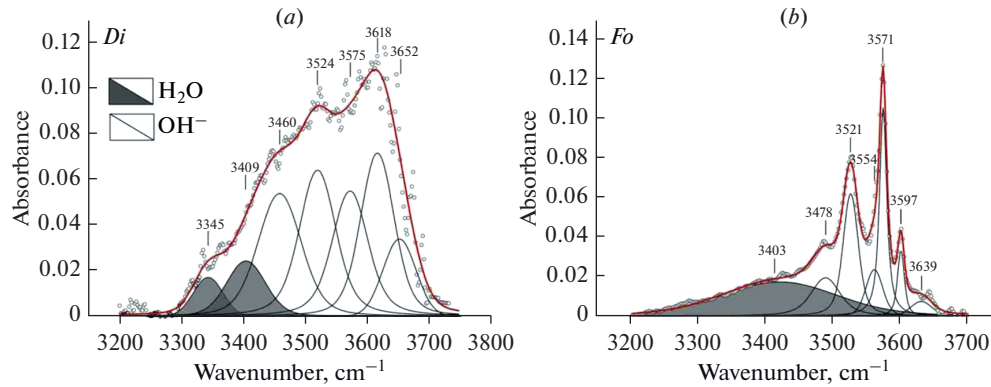


Fig. 1. FTIR spectra of diopside (a) and forsterite (b) in the region of OH⁻ stretching bands (light field) and crystal hydrate water H₂O (dark field). These samples also were studied by STA + QMS.

Рис. 1. Фурье-ИК спектры диопсида (a) и форстерита (b) в области валентных колебаний OH⁻ (светлое поле) и кристаллогидратной воды H₂O (темное поле). Те же образцы были исследованы методом STA + QMS method.

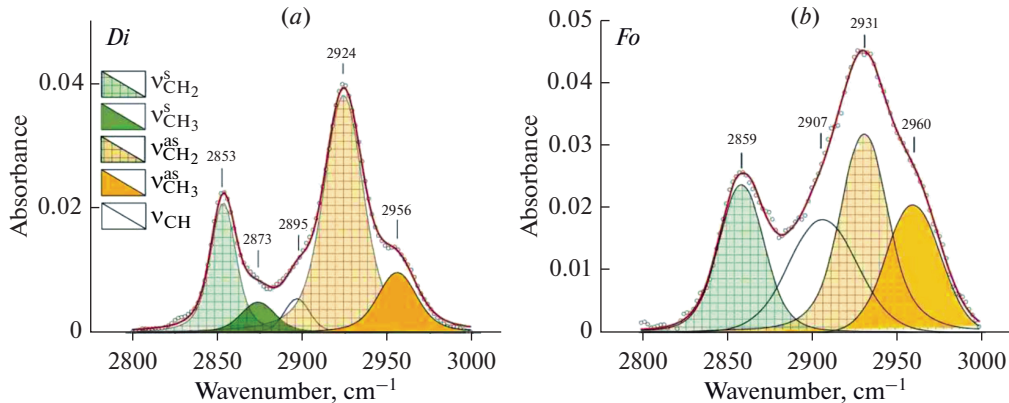


Fig. 2. FTIR spectra of diopside (a) and forsterite (b) in the region of stretching vibration of CH. Symmetric ν^s and antisymmetric ν^{as} vibrations of C–H bond in CH₂ and CH₃ groups. These samples also were studied by STA + QMS.

Рис. 2. Фурье-ИК спектры диопсида (a) и форстерита (b) в области валентных колебаний CH. Симметричные ν^s и антисимметричные ν^{as} колебания связи C–H в CH₂ и CH₃ группах. Те же образцы были исследованы методом STA + QMS method.

According to STA + QMS the thermograms of forsterite and diopside also contain peaks of releasing for m12, m13, m14, m15, m16 and m44, correlated with C, CH, CH₂, CH₃, CH₄, and CO₂, accordingly (Fig. 5, a, b, c, d). The first peaks of releasing for m12, m13, m14, m16, and m44 are located in the temperature range of 500–700 °C, the second region is in the range of 800–1000 °C, and the third region is in the range of 1200–1300 °C. Value of ion current in

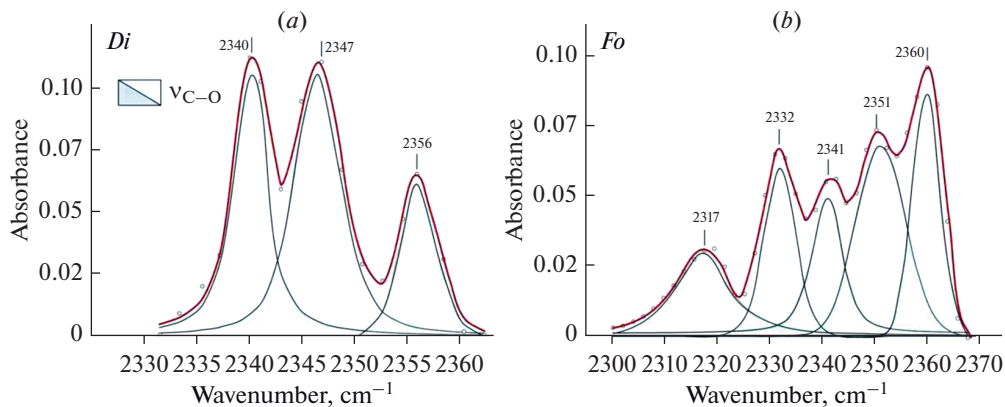


Fig. 3. FTIR spectra of diopside (a) and forsterite (b) in the region of stretching vibration of CO bond. These samples also were studied by STA + QMS.

Рис. 3. Фурье-ИК спектры диопсида (a) и форстерита (b) в области валентных колебаний СО связи. Те же образцы были исследованы методом STA + QMS method.

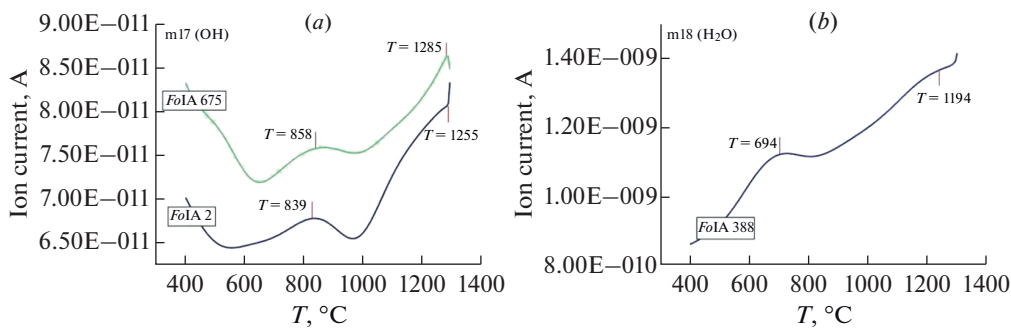


Fig. 4. STA + QMS data for forsterite: (a) curve of eliminating of m17 (OH⁻), (b) curve of eliminating of m18 (H₂O).

Рис. 4. STA + QMS method данные для форстерита: (a) кривая изменения массы m17 (OH⁻), (b) кривая изменения массы m18 (H₂O).

the thermograms for m14, m16, and m44 is more than one for m12, m13, and m15 by 1–2 orders of magnitude, at that IC of diopside sample exceeds slightly ones of forsterite samples. The high temperatures (500–1300 °C) of release of carbon and hydrogen species for gem-quality mineral plates indicate their strong bond with the crystal structure.

The ratios of hydrogen and carbon groups determined by FTIR for unheated samples and STA + QMS analyses for forsterite and diopside at 1300 °C are presented in Table 1. The data of the two methods give comparable results for the proportions of these groups in the forsterite and diopside crystal structures.

Volatiles in minerals of mantle peridotites and pyroxenites. Pyroxenes, forsterites and pyropes from xenoliths of mantle rocks in alkaline basalts and kimberlites of Northwestern Spitsbergen, Mongolia (Dariganga plateau, Tariat depression), Baikal Region (Vitim plateau, Bartoy), Eastern Siberia (“Udachnaya”) have been investigated. Petrological and thermobarometric characteristics of mantle xenoliths are presented in Table 2, compositions of minerals and iron

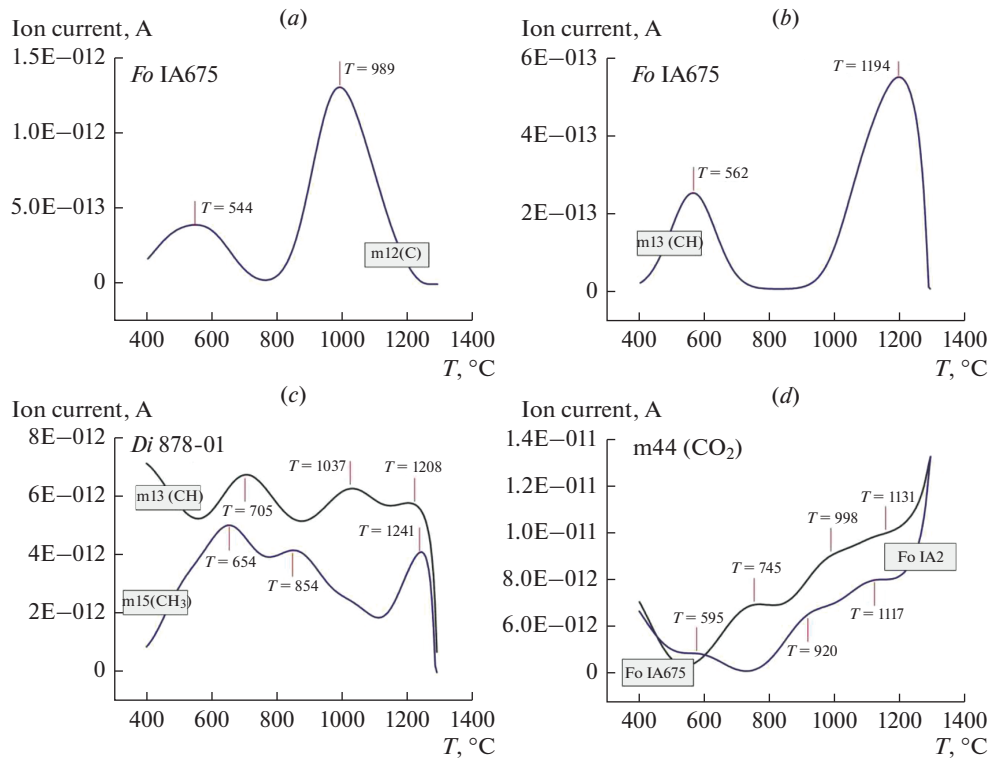


Fig. 5. Curves of eliminating of m12, m13, m15, m44 from forsterite (a, b, d) and diopside (c). (a) m12 (C), (b) m13 (CH), (c) m13 (CH) and m15 (CH₃), (d) 44 (CO₂).

Рис. 5. Кривые изменения масс m12, m13, m15, m44 форстерита (a, b, d) и диопсида (c). (a) m12 (C), (b) m13 (CH), (c) m13 (CH) и m15 (CH₃), (d) 44 (CO₂).

oxidation state published for the first time are presented in Table 3. Compositions of the other samples studied in this paper have been published in (Glebovitsky et al., 2007; Nikitina et al., 2010; Goncharov, Ionov, 2012; Goncharov et al., 2012, 2015).

According to FTIR in the structure of all studied minerals of peridotites and pyroxenites OH⁻ ions (absorption bands in the region of 3750–3450 cm⁻¹) and molecules of H₂O_{cryst} dif-

Table 1. Comparison of fractions of structurally related volatiles (H₂O, CH, CO) in crystal structures of forsterite and diopside from FTIR and STA + QMS

Таблица 1. Сравнение долей H₂O, CH, CO, в кристаллических структурах форстерита и диопсида по данным Фурье-ИК-спектроскопии и метода STA + QMS method

Sample	STA + QMS				FTIR			
	T, °C	H ₂ O ^{miner}	CH ^{miner}	CO ^{miner}	T, °C	H ₂ O ^{miner}	CH ^{miner}	CO ^{miner}
Fo IA388	1300	0.80	0.19	0.01	20	0.85	0.14	0.01
Di 878-001	1300	0.86	0.13	0.01	20	0.88	0.11	0.01

T, °C corresponds to STA + QMS heating temperature and temperature of FTIR experiment. H₂O_{tot} = Σ m17 + m18, CH = Σ m14 + m16, CO = m44. The values of ion currents (IC) to determine the relative shares are normalized to the weight of the plate.

Table 2. Petrological and thermobarometric data for mantle xenoliths from alkali basalts and kimberlites
Таблица 2. Петрологические и термобарометрические данные для мантийных ксенолитов из щелочных базальтов и кимберлитов

Sample	Rock	Modal composition, %					<i>T</i> , °C	<i>P</i> , GPa	$\Delta \text{lg}/\text{O}_2$ (FMQ)	<i>F</i> , %	Reference
		Fo	En	Di	Prp	Spl					
<i>NW Spitsbergen</i>											
2161-71	a	74	14	10	—	2	930	1.9	-1.22	28	1
2162-2	a	74	18	6	—	2	1060	2.4	0.28	29	1
2166-10	a	59	27	11	—	3	730	1.3	-0.44	10	1
2166-11	a	83	9	6	—	2	1030	2.3	-1.44	30	1
2166-18	a	69	19	9	—	3	930	2.0	-0.96	24	1
2166-24	a	60	27	10	—	3	880	1.8	-0.36	13	1
2166-25	a	67	24	7	—	2	1150	2.7	-0.17	22	1
2166-3	a	51	33	13	—	3	910	1.9	-1.06	0	1
2166-8	a	79	11	7	—	3	770	1.5	-0.68	27	1
2166-9	a	63	26	9	—	2	850	1.7	-0.78	15	1
Shp2	a	62	27	10	—	1	950	2.0	-1.16	11	1
Shp10	b	29	61	—			1010	2.1	n.d.	n.d.	1
Shp13	c	16	68	2	1		1310	3.3	n.d.	n.d.	1
Shp16	d		52	47	1		1080	2.3	n.d.	n.d.	1
Shp19	d		61	37	2		n.d.	n.d.	n.d.	n.d.	1
Shp1b	d	n.d.	n.d.	n.d.	n.d.		n.d.	n.d.	n.d.	n.d.	1
Shp4	d	n.d.	2	65	33	n.d.	n.d.	n.d.	n.d.	n.d.	1
<i>Dariganga plateau</i>											
8520/11	a	69	18	12	—	1	1210	3.5	-1	21	2
8520/40	a	70	19	10	—	1	1120	3.3	-1.12	25	2
502b-105	a	70	19	10	—	1	n.d.	n.d.	n.d.	n.d.	2
<i>Tariat depression</i>											
8530/14	a	65	24	9	—	2	1100	3.0	-1.62	34	2
652a	a	62	21	15	—	2	1130	3.1	-0.3	n.d.	2
647	a	62	21	15	—	2	1290	3.4	-1.01	n.d.	2
SHC	a	62	21	15	—	2	1190	3.0	-1.04	n.d.	2
878-01	a	62	21	15	—	2	1230	3.2	-0.76	n.d.	2
210-u/76	a	62	21	15	—	2	1280	3.3	-0.83	n.d.	2
SHCst	a	62	21	15	—	2	1200	3.1	n.d..	n.d.	2
<i>Vitim plateau</i>											
Vt4	e	66	10	15	8	1	1300	3.8	-1.6	13	2
Vt5	f	60	16	14	10	0	1360	4.1	-2.35	9	2
Vt7	e	61	19	11	8	1	n.d..	n.d..	-4.49	13	2
Vt8	e	56	16	14	13	1	1340	3.8	-2.68	5	2
Vt11	f	65	18	15	—	2	1240	3.4	-0.13	13	2
Vt12	f	74	14	10	—	2	1330	3.9	-1.12	25	2
Vt15	e	63	22	9	5	1	1440	4.3	-0.71	20	2

Table 2. (Contd.)

Sample	Rock	Modal composition, %					<i>T</i> , °C	<i>P</i> , GPa	$\Delta g/fO_2$ (FMQ)	<i>F</i> , %	Reference
		Fo	En	Di	Prp	Spl					
<i>Bartoi</i>											
IA1	a	94	4	2	—	—	n.d.	n.d.	n.d.	52	2
IA2	a	95	1	4	—	—	n.d.	n.d.	n.d.	51	2
IA3	a	93	6	1	—	—	n.d.	n.d.	n.d.	53	2
IA2a	a	75	12	13	—	—	n.d.	n.d.	n.d.	23	2
IA675	a	89	6	5	—	—	n.d.	n.d.	n.d.	48	2
<i>Udachnaya pipe</i>											
87/114	g	n.d.	n.d.	n.d.	n.d.	n.d.	1250	5.2	n.d.	n.d.	2
87/70	g	n.d.	n.d.	n.d.	n.d.	n.d.	1230	5.4	n.d.	n.d.	2
IA180	f	n.d.	n.d.	n.d.	n.d.	n.d.	n.d.	n.d.	n.d.	n.d.	2
IA215	f	n.d.	n.d.	n.d.	n.d.	n.d.	n.d.	n.d.	n.d.	n.d.	2
IA272	f	n.d.	n.d.	n.d.	n.d.	n.d.	n.d.	n.d.	n.d.	n.d.	2
IA388	f	79	13	7	1	n.d.	1300	5.2	n.d.	40	2
Y-1	f	76	15	7	2	n.d.	1320	5.2	-0.5	36	2
Y-3	f	65	16	12	7	n.d.	1320	5.1	-3	13	2
Y-4	f	63	10	21	6	n.d.	1200	4.7	-1.04	11	2

Rock types: (a) spinel lherzolites, (b) websterites, (c) garnet websterites, (d) garnet clinopyroxenites, (e) garnet-spinel lherzolites, (f) garnet-lherzolites, (g) garnet harzburgites. References: (1) Goncharov et al., 2015; (2) this study. *F* corresponds to partial melting degree. Mineral abundances are calculated by the least square method on the basis of the whole-rocks and minerals (Goncharov et al., 2012). For temperature and pressure calculations see the text. n.d. means not determined. To estimate temperatures and pressures, we used modified garnet-orthopyroxene thermobarometer and clinopyroxene- orthopyroxene geothermometer (Nikitina et al., 2010).

fering on hydrogen bond energy (absorption bands in the field of 3450–3000 cm⁻¹ and 1680–1530 cm⁻¹) are presented. Fig. 1 shows typical FTIR spectra of diopside (*a*) and forsterite (*b*), Fig. 6 shows spectra of enstatite (*a*), and pyrope (*d*) in the region of stretching vibrations of OH⁻ bonds and H₂O_{cryst} with fitting of these spectra using mixed functions of Gauss and Lorentz “Voigt area G/L”. The spectral region of 3450–3000 cm⁻¹ assign to stretching vibrations of crystal hydrate water H₂O_{cryst} – i.e. water molecules that have not lost their chemical individuality and form relatively weak hydrogen bonds (Lazarev, 1995). Spectra of the studied minerals have an absorption band within 1680–1530 cm⁻¹ (Fig. 7), that corresponds to bending vibration of crystal hydrate water (δ H₂O) and is an important indicator of its presence in the structure (Lazarev, 1995). Two absorption bands are observed in the diopside (*a*) and enstatite (*b*) spectra: 1564 and 1641 cm⁻¹ and 1587 and 1661 cm⁻¹, respectively. In the spectrum of forsterite (*c*) – one band is 1672 cm⁻¹. We assume that the presence of two bands is related to more complex structures of diopside and enstatite compared to the structure of forsterite and the variety in the population of octahedron and tetrahedron cations.

The region of 3650–3450 cm⁻¹ is characteristic for stretching vibrations of hydroxyl ion. Spectra in this region are different for minerals of different composition due to the effect of differences in the occupation of cations of the first and second coordination spheres on the stretching vibrations of the hydroxyl ion OH⁻. The infrared spectra of minerals contain absorption bands of OH⁻ within the following ranges of wavenumbers:

Table 3. Major element composition (wt %) and iron oxidation state of minerals from mantle peridotite xenoliths

Таблица 3. Химический состав (мас. %) и степень окисления железа минералов из ксенолитов мантийных перидотитов

Sam- ple	Miner- al	SiO ₂	TiO ₂	Al ₂ O ₃	Cr ₂ O ₃	FeO	Fe ₂ O ₃	MnO	MgO	CaO	Na ₂ O	K ₂ O	NiO	Total	Fe ³⁺ / ΣFe
652a	Di	51.70	0.70	5.60	1.00	2.10	0.80	0.20	17.10	20.00	1.40	—	—	100.60	0.250
652a	En	53.40	0.20	6.00	0.40	5.90	0.50	0.20	32.70	0.90	—	—	—	100.10	0.080
652a	Fo	40.40	—	—	—	9.70	0.10	0.10	49.40	0.10	—	—	0.40	100.40	0.010
647	Di	50.66	0.25	6.76	0.93	2.03	0.74	0.17	16.36	20.68	—	—	1.24	99.82	0.247
647	En	54.19	—	5.45	0.46	5.77	0.18	0.16	32.96	0.86	—	—	—	100.03	0.027
647	Fo	40.42	—	—	—	8.90	0.40	0.20	49.70	—	—	—	0.36	99.94	0.040
SHC	Di	50.79	0.66	7.43	0.75	1.84	0.50	0.17	15.14	20.74	2.07	—	—	100.09	0.197
SHCst	Di	50.80	0.70	7.20	0.70	1.80	0.50	—	14.90	20.90	2.10	—	—	99.70	0.210
SHCst	En	55.10	0.20	4.30	0.30	5.50	0.20	—	34.00	0.50	—	—	—	100.10	0.040
SHCst	Fo	40.70	—	—	—	9.30	—	0.20	49.90	—	—	—	0.30	100.40	—
IA1	Di	51.51	0.16	4.48	1.36	2.48	0.17	0.08	16.34	22.44	0.78	0.05	—	99.85	0.058
IA1	En	56.09	0.07	3.92	0.76	5.44	0.15	0.15	31.71	1.22	0.05	0.01	—	99.57	0.024
IA1	Fo	42.02	0.02	—	0.02	8.55	—	0.12	48.26	0.11	0.12	0.02	0.43	99.67	—
IA2	Di	51.11	0.49	6.53	0.82	2.40	0.39	0.09	15.89	20.69	1.10	0.01	—	99.52	0.127
IA2	En	55.60	0.15	5.31	0.50	4.97	0.25	0.15	31.54	1.12	0.17	0.02	—	99.78	0.043
IA2	Fo	42.19	0.03	—	0.05	8.52	—	0.07	48.21	0.11	0.06	0.01	0.42	99.67	—
IA3	Di	50.79	0.52	6.18	1.26	2.48	0.57	0.14	15.28	21.29	1.29	0.01	—	99.81	0.171
IA3	En	55.71	0.14	4.79	0.73	5.96	0.18	0.14	31.03	1.16	0.03	0.01	—	99.88	0.026
IA3	Fo	42.12	0.03	—	0.05	9.44	—	0.12	47.64	0.09	0.01	0.03	0.41	99.94	—
IA2a	Di	51.00	0.50	7.20	1.00	2.70	0.80	0.10	14.40	20.60	1.70	0.00	—	100.00	0.218
IA2a	En	55.30	0.10	5.00	0.50	6.30	0.20	0.20	30.90	1.00	0.10	—	—	99.60	0.029
IA2a	Fo	41.40	0.00	0.00	0.10	10.10	0.00	0.20	47.30	0.10	0.10	0.00	0.50	99.70	—
IA675	Di	51.85	0.11	4.56	1.25	2.41	0.19	0.12	17.43	20.81	0.85	0.03	0.10	99.71	0.066
IA675	En	55.11	0.06	4.12	0.81	5.08	0.14	0.12	32.77	1.15	0.05	—	0.07	99.48	0.024
IA675	Fo	41.11	0.04	—	0.05	8.11	—	0.14	49.51	0.10	0.03	0.01	0.49	99.59	—
IA180	Di	55.20	0.20	2.00	0.50	4.40	—	0.10	17.10	20.00	1.50	—	0.10	101.10	0.046
IA180	Fo	39.80	—	—	—	13.10	—	0.10	46.50	—	—	—	0.20	99.70	0.160
IA215	Di	54.80	0.40	2.40	1.10	3.80	—	0.10	18.40	17.00	1.70	0.00	—	99.70	0.024
IA215	En	56.80	0.20	0.90	0.20	5.60	—	0.10	34.00	1.00	0.20	—	0.10	99.10	—
IA215	Fo	41.00	—	—	—	9.60	—	0.10	49.80	—	—	—	0.40	100.90	—
IA215	Prp	41.80	0.70	20.90	2.70	7.80	—	0.20	21.60	4.40	0.10	—	—	100.20	—

The chemical analysis of minerals has been performed by SEM-EDX method and the valence state of iron and the Fe³⁺/ΣFe ratio has been determined using Mössbauer spectroscopy at the Institute of Precambrian Geology and Geo-chronology RAS. Here we present the unpublished mineral compositions. For the composition of other studied samples see (Glebovitsky et al., 2009; Goncharov, Ionov, 2012; Goncharov et al., 2012; Goncharov et al., 2015).

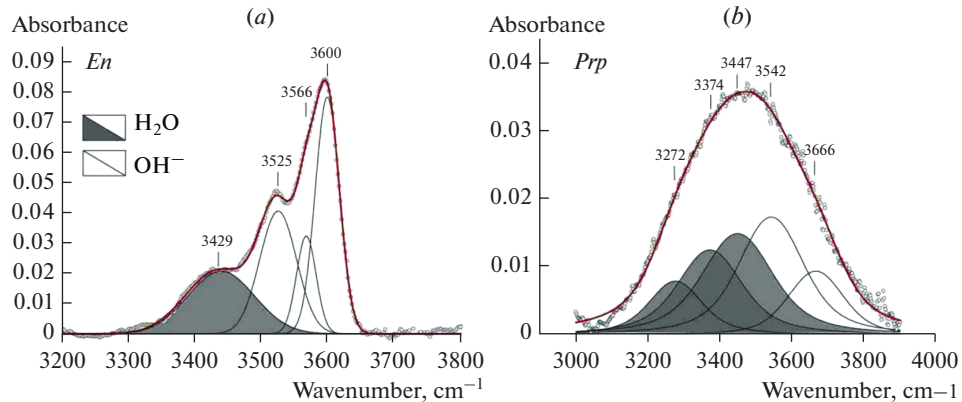


Fig. 6. FTIR spectra of enstatite (a) and pyrope (b) in the region of OH⁻ stretching bands (light field) and crystal hydrate water H₂O (dark field).

Рис. 6. Фурье-ИК спектры энstatита (a) и пиропа (b) в области валентных колебаний OH⁻ (светлое поле) и кристаллогидратной воды H₂O (темное поле).

diopside: OH⁻ 3650–3600, 3570–3520, 3470–3450 cm⁻¹; H₂O_{cryst} 3400–3300 cm⁻¹;
enstite: OH⁻ 3600–3560, 3530–3520, 3490–3480 cm⁻¹; H₂O_{cryst} 3420–3310 cm⁻¹;
forsterite: OH⁻ 3640–3590, 3570–3550, 3540–3520, 3490–3480 cm⁻¹; H₂O_{cryst} 3450–3200 cm⁻¹;
pyrope: OH⁻ 3670–3660, 3550–3530 cm⁻¹, H₂O_{cryst} 3450–3270 cm⁻¹.

DISCUSSION

The most important points affecting the accuracy of determination of the volatile content in the structure of NAMs are calibrations and use of oriented grains in polarized light. Generally, calibrations for quantity of the water content in the crystal structure by FTIR are made with other methods for samples with a specific composition. The calibration must be performed by alternative method for each mineral, but it is mostly impossible. The main errors in determining the content of structure-related water in minerals arise from the use of calibrations made for minerals whose compositions differ from those studied. In addition, it is necessary to exclude the possibility of additional contribution of water in microcracks or in fluid microinclusions in a single crystal of mineral.

Furthermore, there are no reliable data on possible orientations of OH⁻ ion in NAMs structures which are changing depend on coordination environment. In the experiments with the absorption of polarized radiation, the only possible transitions take place when the direction of OH⁻ dipole vector coincides with the direction of polarized-wave vector. If the direction of dipole vector in the crystal that is used in the experiment with polarized light is not parallel to the direction of radiation, determination of integral intensity of absorption bands will be incorrect. The orientation of hydroxyl ion (angle of dipole inclination) is also changed in dependence on coordination environments as determined, such as for micas (Rousseaux et al., 1972; Ponomarev, Lapides, 1988, 1990). Various orientations of OH⁻ dipole are discussed for crystal structures of diopside (Ingrin et al., 1989; Skogby et al., 1990) and olivine (Koch-Müller et al., 2006) and are interpreted as distinct hydrogen positions in structures of minerals. Therefore, the use of polarized radiation only for three main crystallographic directions cannot provide full information about the orientation of OH⁻ ion in the crystal structure that

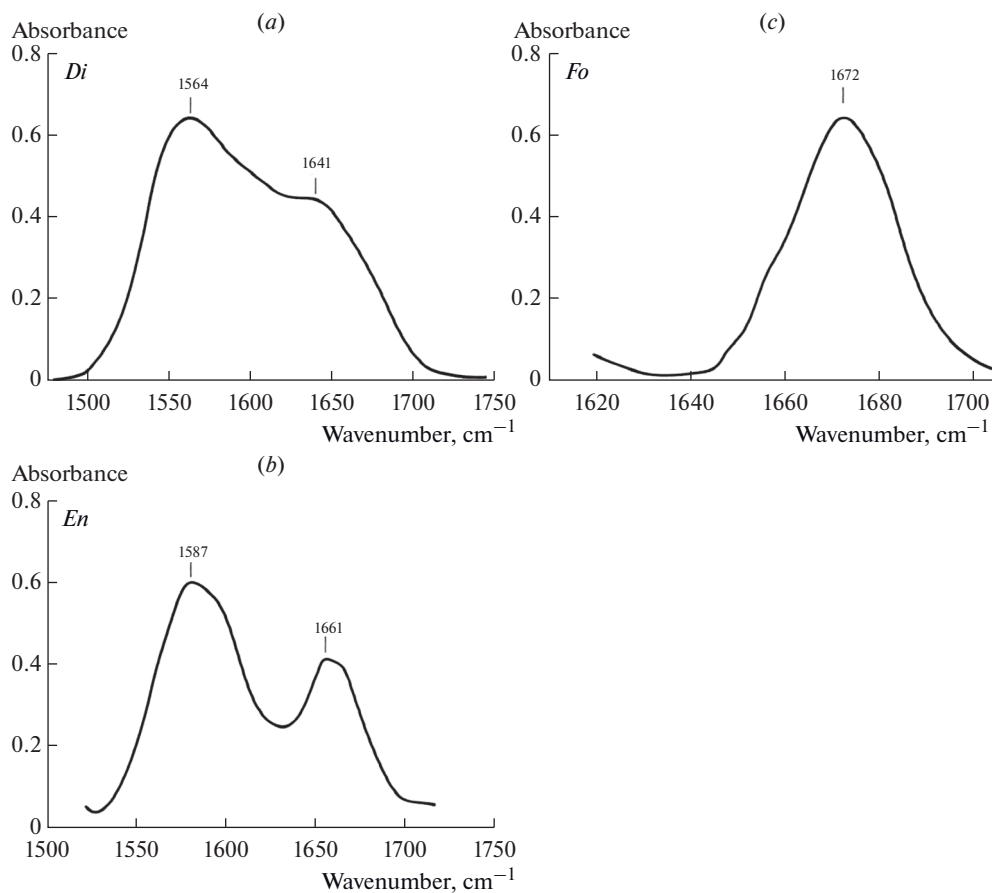


Fig. 7. FTIR spectra of diopside (a), enstatite (b), forsterite (c) in the region of deformation vibration of crystal hydrate H_2O .

Рис. 7. Фурье-ИК спектры диопсида (a), энстатита (b), форстерита (c) в области деформационных колебаний кристаллогидратной воды H_2O .

reduces the accuracy of determination of the integral intensity of absorption bands. According to our estimates, accuracy of determination of the water content in the NAMs structure by FTIR is $\pm 30\%$, which is in agreement with estimates of other researchers (Koch-Müller et al., 2006; Withers, Hirschmann, 2008; Yang et al., 2008). The separation of optically pure grains of mantle minerals from xenoliths and their orientation along crystallographic axes are difficult and, therefore, the method of Kovács et al. (2008) and Sambridge et al. (2008) for the study of unoriented anisotropic grains of minerals in unpolarised IR light allows to determine the concentrations of structural hydroxyl accurately.

Previously (Goncharov et al., 2015), it has been found that the water content in pyroxenes and forsterite from central and edge zones of xenoliths with the total content of structure-related water $\text{H}_2\text{O}_{\text{miner}} = \text{OH}^- + \text{H}_2\text{O}_{\text{cryst}}$ in each mineral from these parts is practically equal. That testifies to preservation of this water during the ascent of xenoliths to the surface. Water in the diopside crystal structure is in the form of OH^- ions predominantly, in enstatite of the

Table 4. Calculated OH⁻, H₂O_{cryst}, H₂O^{miner} content and H₂O, CH, CO parts the crystal structure of studied minerals in peridotites and pyroxenites from kimberlites and basalts

Таблица 4. Содержание OH^- , $\text{H}_2\text{O}_{\text{cryst}}$, $\text{H}_2\text{O}_{\text{пшс}}$ и доли H_2O , CH , CO в кристаллических структурах минералов ксенолитов мантийных периодитов и пироксенитов из базальтов и кимберлитов

Sample	Content, ppm			Parts			Content, ppm			Parts			Parts			Parts		
	OH ⁻	H ₂ O _{cryst}	H ₂ O _{miner}	H ₂ O	CH	CO	OH ⁻	H ₂ O _{cryst}	H ₂ O _{miner}	H ₂ O	CH	CO	OH ⁻	H ₂ O _{cryst}	H ₂ O _{miner}	H ₂ O	CH	CO
	Di			En												Fo		
2161-7-1	119	50	169	0.98	0.02	0.00	25	34	59	0.99	0.01	0.00	3	15	18	0.92	0.03	0.05
2161-7-2	112	149	261	0.94	0.06	0.00	26	32	58	0.94	0.02	0.04	7	5	12	0.50	0.19	0.30
2161-7-4	98	61	159	0.97	0.02	0.01	22	27	49	0.87	0.03	0.10	6	14	20	0.36	0.46	0.18
2162-2	162	40	202	0.94	0.02	0.04	24	29	53	0.93	0.03	0.04	4	11	15	0.79	0.06	0.15
2166-10	104	84	188	0.97	0.03	0.00	14	15	29	0.97	0.02	0.01	13	29	42	0.96	0.03	0.01
2166-11	104	108	212	0.97	0.03	0.00	22	28	50	0.86	0.14	0.00	3	5	8	0.55	0.35	0.10
2166-18	108	74	182	0.99	0.00	0.01	28	23	51	0.96	0.03	0.01	8	16	24	0.86	0.10	0.04
2166-23	168	225	393	0.99	0.01	0.00	—	—	—	—	—	—	5	23	28	0.91	0.04	0.04
2166-24	94	65	159	0.97	0.03	0.00	24	21	45	0.99	0.01	0.00	4	4	8	0.63	0.23	0.13
2166-25	91	51	142	0.97	0.03	0.00	30	28	58	0.95	0.05	0.00	8	12	20	0.46	0.53	0.01
2166-27	111	58	169	0.99	0.00	0.01	21	18	39	1.00	0.00	0.00	2	3	5	0.75	0.15	0.10
2166-3	60	51	111	0.98	0.01	0.01	12	9	21	0.96	0.01	0.03	3	13	16	0.67	0.18	0.15
2166-6	89	66	155	0.96	0.04	0.00	—	—	—	—	—	—	8	7	15	0.38	0.58	0.04
2166-8	121	49	170	0.98	0.01	0.01	26	22	48	0.98	0.01	0.01	7	31	38	0.75	0.20	0.05
2166-9	117	128	245	0.99	0.01	0.00	32	30	62	0.99	0.00	0.01	6	7	13	0.89	0.05	0.06
Shp2	95	80	177	1.00	0.00	0.00	24	16	40	1.00	0.00	0.00	2	13	15	0.82	0.17	0.01
Shp2a	88	84	172	0.95	0.04	0.01	26	19	45	0.99	0.00	0.01	11	16	27	0.95	0.03	0.02
Shp10	128	113	241	1.00	0.00	0.00	—	—	—	—	—	—	—	—	—	—	—	—
Shp13	121	166	287	1.00	0.00	0.00	—	—	—	—	—	—	—	—	—	—	—	—
Shp16	166	94	260	1.00	0.00	0.00	—	—	—	—	—	—	—	—	—	—	—	—
Shp19	121	95	216	0.97	0.01	0.02	—	—	—	—	—	—	—	—	—	—	—	—
Shp1b	145	97	242	1.00	0.00	0.00	45	25	70	1.00	0.00	0.00	—	—	—	—	—	—
Shp4	165	71	236	0.99	0.01	0.00	—	—	—	—	—	—	—	—	—	—	—	—
8520/11	144	70	214	0.96	0.03	0.01	32	77	109	0.99	0.01	0.00	18	69	87	0.94	0.02	0.04
8520/40	79	19	98	0.94	0.04	0.02	20	42	62	0.97	0.01	0.02	9	20	29	0.95	0.05	0.00
502b-105	19	20	39	0.91	0.09	0.00	10	22	32	0.90	0.10	0.00	21	47	68	0.84	0.10	0.06
8530/14	38	11	49	0.93	0.02	0.05	10	19	29	0.93	0.02	0.05	6	1	7	0.49	0.33	0.18
652a	141	101	242	0.95	0.05	0.00	62	135	197	0.95	0.02	0.02	16	32	48	0.92	0.08	0.00
647	71	79	150	0.94	0.03	0.03	39	148	187	0.99	0.00	0.01	105	133	105	0.87	0.11	0.02

Table 4. (Contd.)

Sample	Content, ppm		Parts			Content, ppm			Parts			Content, ppm			Parts				
	OH ⁻	H ₂ O _{cryst}	H ₂ O _{miner}	H ₂ O	CH	CO	OH ⁻	H ₂ O _{cryst}	H ₂ O _{miner}	H ₂ O	CH	CO	OH ⁻	H ₂ O _{cryst}	H ₂ O _{miner}	H ₂ O	CH	CO	
Di																			
III	145	78	223	0.69	0.30	0.01	30	76	106	0.90	0.08	0.02	13	82	95	0.58	0.36	0.05	
878-01	110	35	145	0.88	0.11	0.01	40	84	124	0.93	0.05	0.02	61	30	91	0.92	0.05	0.03	
210-Y/76	88	102	190	1.00	0.00	0.00	24	63	86	0.93	0.05	0.02	64	168	232	0.84	0.15	0.01	
SHC _{St}	130	73	203	0.97	0.02	0.01	36	84	120	0.98	0.00	0.02	20	89	109	0.81	0.18	0.02	
Vt4	98	37	135	0.99	0.01	0.00	35	65	100	0.88	0.00	0.12	8	16	24	0.52	0.46	0.03	
Vt5	143	132	275	0.95	0.03	0.02	29	59	88	0.93	0.07	0.01	22	29	51	0.87	0.11	0.02	
Vt7	176	54	230	0.88	0.11	0.01	49	113	162	0.89	0.10	0.01	17	39	56	0.79	0.17	0.03	
Vt8	99	87	186	0.96	0.03	0.01	26	50	76	0.95	0.05	0.00	39	164	203	0.96	0.02	0.02	
Vt11	158	89	247	0.97	0.02	0.01	72	151	223	0.86	0.13	0.01	38	88	126	0.80	0.18	0.02	
Vt12	216	118	334	0.97	0.02	0.01	42	109	151	0.83	0.17	0.00	45	135	180	0.84	0.15	0.02	
Vt15	83	61	144	0.96	0.04	0.00	22	40	63	0.92	0.06	0.02	2	12	14	0.29	0.71	0.00	
IA1	69	21	90	0.96	0.04	0.00	23	3	26	1.00	0.00	0.00	2	1	3	0.20	0.11	0.69	
IA2	60	55	115	0.89	0.00	0.11	15	24	39	0.90	0.00	0.10	10	20	30	0.97	0.03	0.00	
IA2a	234	48	282	0.98	0.01	0.01	34	35	69	1.00	0.00	0.00	7	11	18	0.70	0.00	0.30	
IA3	77	41	118	0.94	0.02	0.04	28	24	52	1.00	0.00	0.00	15	12	27	0.75	0.21	0.04	
IA4	112	46	158	0.91	0.02	0.07	36	37	73	0.93	0.00	0.07	13	21	34	0.97	0.00	0.03	
IA675	55	10	65	0.83	0.17	0.00	20	10	30	0.95	0.05	0.00	4	6	10	0.77	0.00	0.23	
IA5	118	57	175	0.82	0.16	0.02	27	41	68	1.00	0.00	0.00	12	6	18	1.00	0.00	0.00	
87-114	-	-	-	-	-	-	106	81	187	1.00	0.00	0.00	-	-	-	-	-	-	
87-70	-	-	-	-	-	-	52	28	80	0.99	0.00	0.01	-	-	-	-	-	-	
IA180	106	24	130	0.96	0.02	0.02	-	-	17	0.89	-	-	100	0	100	0.98	0.00	0.02	
IA215	102	92	194	0.99	0.01	0.01	12	5	-	-	-	-	95	65	160	0.99	0.00	0.01	
IA272	148	39	187	0.92	0.07	0.01	-	-	-	-	-	-	70	36	106	0.90	0.09	0.01	
IA388	28	15	43	0.80	0.10	0.09	16	19	35	0.97	0.03	0.01	86	28	114	0.85	0.14	0.01	
Y-1	26	24	51	0.74	0.20	0.06	12	12	24	0.91	0.07	0.02	46	25	71	0.94	0.02	0.04	
Y-3	48	58	106	0.96	0.03	0.01	15	7	22	0.98	0.02	0.00	74	18	92	1.00	0.00	0.00	
Y-4	37	14	51	0.94	0.05	0.01	15	8	23	0.98	0.01	0.01	61	6	67	0.95	0.02	0.03	

Table 5. Calculated OH⁻, H₂O_{cryst}, H₂O^{miner} contents and H₂O, CH, CO parts in the crystal structure of studied pyrope from mantle xenoliths of NW Spitsbergen, Vitim and Udachnaya pipe

Таблица 5. Содержание OH⁻, H₂O_{cryst}, H₂O^{miner} и доли H₂O, CH, CO в кристаллической структуре пиропа из мантийных ксенолитов СЗ Шпицбергена, Витима и трубы Удачной

Sample	Content, ppm			Parts		
	OH ⁻	H ₂ O _{cryst}	H ₂ O ^{miner}	H ₂ O	CH	CO
Peridotites						
<i>Vitim plateau</i>						
Vt4	129	213	342	0.89	0.07	0.04
Vt5	8	25	33	0.87	0.13	—
<i>Udachnaya pipe</i>						
Y-1	23	32	55	0.81	0.16	0.03
Y-3	13	31	44	0.95	—	0.05
Y-4	33	86	119	1.00	—	—
IA215	21	36	57	0.81	0.16	0.02
87-70	6	2	8	0.6	0.37	0.03
Pyroxenites						
<i>NW Spitsbergen</i>						
Shp16	—	38	38	1.00	—	—
Shp18	—	34	34	1.00	—	—
Shp19	20	12	32	1.00	—	—
Shp1b	84	80	164	0.97	0.03	—

Tariat depression, Dariganga and Vitim plateaus content of crystal hydrate form exceeds hydroxyl one, in the structure of enstatite of Bartoy and pipe “Udachnaya” hydroxyl form either slightly exceeds crystal hydrate one or content of both forms is the same (Table 4). Crystal hydrate form prevails in forsterite and pyrope except forsterite of Bartoy and pipe “Udachnaya”, in which structure the hydroxyl form dominates (Tables 4 and 5).

Infrared spectra of the majority of studied minerals show absorption bands of stretching vibrations of CH and CO groups that can testify entry of one or more forms of carbon groups into the crystal structure (Figs. 2, 3, 8, 9). The research shows that the absorption bands of CH and CO groups are present in all IR spectra of forsterite and in some spectra of pyroxenes and pyropes. Ratio of water and carbon in structures of all studied minerals has been determined (equation 1). The estimates are semi-quantitative, but give an idea of the ratio of these volatiles in structures of studied minerals. Fractions of CH in majority of diopside ranges from 0.01 to 0.05, one of CO varies from 0 to 0.05 (Table 4). Fractions of CH and CO in the majority of enstatite are 0–0.05. Forsterite characterized with the decrease of the water content of volatiles and increase of CO and CH contents. Fractions of CH and CO for half of forsterites samples range from 0 to 0.35. In some samples from Vitim and Spitsbergen share of CH is 0.46–0.71. Fractions of CO in forsterite IA1 (Bartoy) is 0.69. Fractions of carbon compounds in forsterite are significant in comparison with the pyroxenes. Pyropes contain predominantly water composition of volatiles with fractions of CO and CH from 0 to 0.05. In a few pyrope samples (Vitim, Udachnaya) fractions of CH is 0.13 – 0.37 (Table 5). Portions of water and carbon testify to predominantly water composition of volatiles in the structure of the majority of studied minerals. The presence of hydrogen and carbon in the form of OH⁻ ions, molecules H₂O_{cryst}, CO₂, CH, CH₂, CH₃ in the structures of forsterite and diopside from mantle peridotites is proved using FTIR microspectroscopy and STA + QMS analysis. In FTIR spectra and STA + QMS thermograms for the same mineral plates are present absorption bands of stretching vibrations and the peaks of the selection of masses belonging to the same hydrogen and carbon

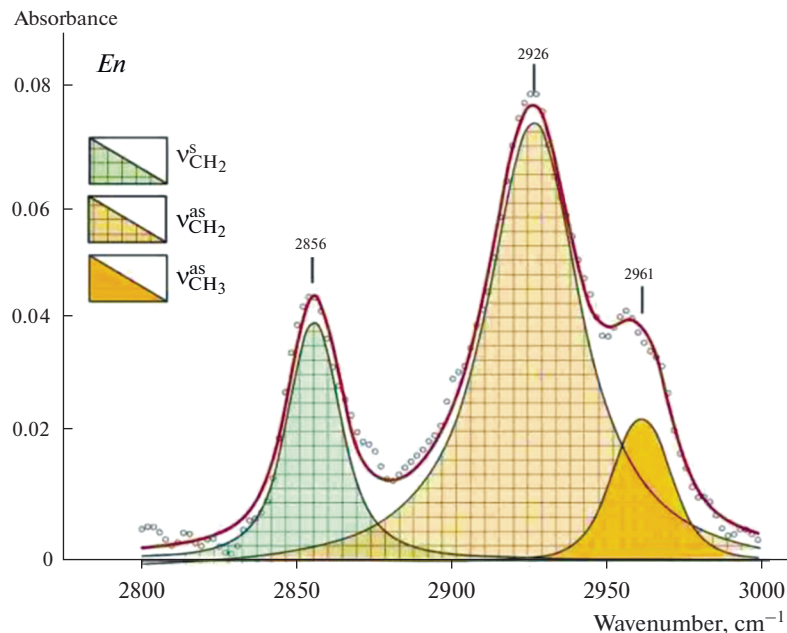


Fig. 8. FTIR spectrum of enstatite in the region of stretching vibration of CH bond. Symmetric ν^{s} and antisymmetric ν^{as} vibrations of C–H bond in CH_2 and CH_3 groups.

Рис. 8. Фурье-ИК спектр энстатита в области валентных колебаний СН. Симметричные ν^{s} и антисимметричные ν^{as} колебания связи С–Н в CH_2 and CH_3 группах.

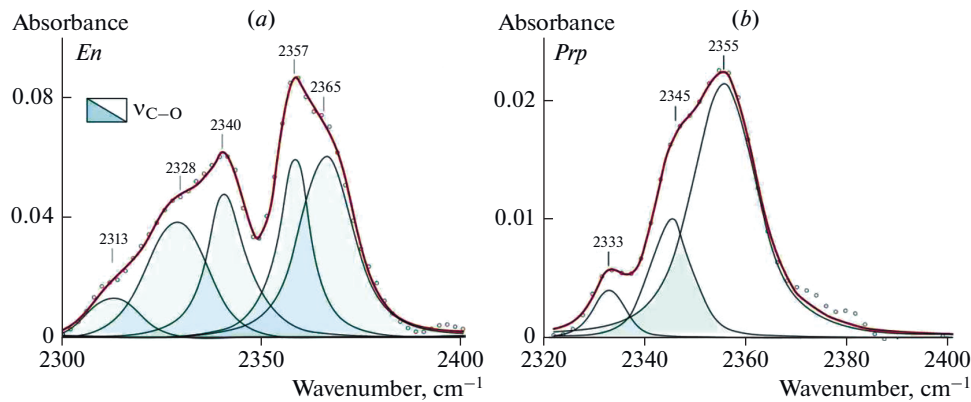


Fig. 9. FTIR spectra of enstatite (a) and pyrope (b) in the region of stretching vibration of CO bond.

Рис. 9. Фурье-ИК спектры энстатита (a) и пиропа (b) в области валентных колебаний СО связи.

forms, and the water component ($\text{OH}^- + \text{H}_2\text{O}_{\text{cryst}}$) is the predominant component among the volatiles. This makes it possible to use the FTIR method as a more convenient method for the study of large arrays of samples, in particular xenoliths of mantle rocks, carried out by basalt and kimberlite magmas.

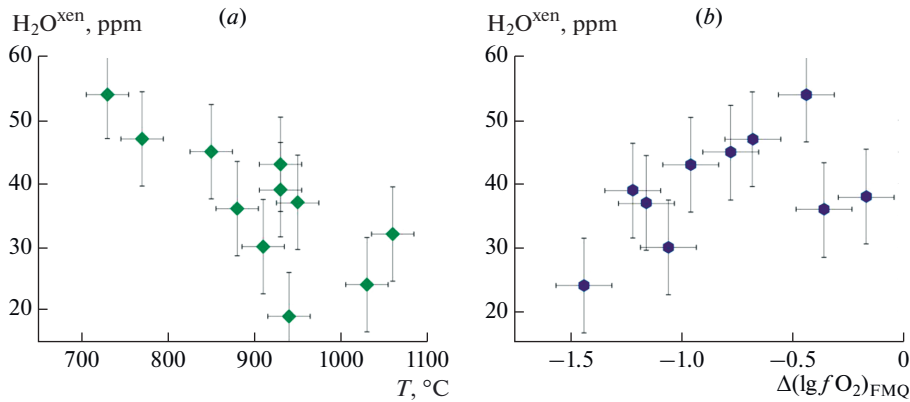


Fig. 10. Dependence of total water content (H_2O^{xen}) in Spitsbergen peridotite xenoliths vs temperature (a) and the oxygen fugacity (b).

Рис. 10. Зависимость содержания воды (H_2O^{xen}) в ксенолитах Шпицбергена от температуры кристаллизации (a) и фугитивности кислорода $\Delta(\lg f O_2)_{FMQ}$ (b).

Volatiles in xenoliths and thermodynamic equilibrium conditions. The total water content (H_2O^{xen} , ppm) and fractions of volatile components (H_2O , CH , and CO) for each xenolith calculated with regard to mineral abundances are given in Table 6. H_2O^{xen} varies from 10 to 200 ppm and is the main volatile component in xenoliths. In order to identify the factors that influencing water solubility in NAMs structures and to determine preservation conditions of water, we have studied mineral assemblages, compositions of coexisting minerals and iron oxidation state in spinel and pyrope, that allows determining thermodynamic conditions (T , P , f_{O_2}) for studied samples. To estimate temperature and pressure we used modified garnet-orthopyroxene thermobarometer and clinopyroxene-orthopyroxene geothermometer (Nikitina et al., 2010). Calculation of the oxygen fugacity has been performed with olivine-orthopyroxene-spinel (Wood, 1991), and garnet-olivine-orthopyroxene (Gudmundsson, Wood, 1995) oxygen geobarometers.

Equilibrium conditions of mineral associations of peridotites are given in Table 2. Estimates of oxygen fugacity are given in relation to fayalite-magnetite-quartz (FMQ) oxygen buffer at the same T and P [$\Delta(\lg f O_2)_{FMQ} = (\lg f O_2 - \lg f O_2^{FMQ})$]. Volatiles are present in the crystal structure of minerals formed in the range of temperatures from 750 to 1450 °C, pressures from 1.5 to 5.5 GPa at the oxygen fugacity $\Delta \lg f O_2^{FMQ}$ which varied from -4.5 to +0.3 (Table 2). This testify to high strength of their connection with crystal lattices of studied NAMs. As an example, we present dependence of the water content in xenoliths of Spitsbergen on crystallization temperature, $\Delta(\lg f O_2)_{FMQ}$, and partial melting degree (F , %) (Figs. 10, 11). The water content in peridotite xenoliths of Spitsbergen decreases with temperature (Fig. 10, a) and increases with rise in the oxygen fugacity (Fig. 10, b). However, the clear dependence of the water content in the xenoliths (H_2O^{xen}) on parameters of the equilibrium of minerals (T , P , f_{O_2}) for all studied regions has not been stated. Degree of partial melting of peridotite (F) has been calculated on the basis of data of composition of xenoliths according to equation (Nikitina et al., 2017):

Table 6. Calculated $\text{H}_2\text{O}^{\text{xen}}$ content and H_2O , CH , CO parts in studied mantle peridotite xenoliths
Таблица 6. Содержание $\text{H}_2\text{O}^{\text{xen}}$ и соотношение долей H_2O , CH , CO в ксенолитах мантийных перидотитов

Sample	$\text{H}_2\text{O}^{\text{xen}}$, ppm	Parts			Reference
		H_2O	CH	CO	
2161-71	39	0.94	0.02	0.04	1
2162-2	32	0.83	0.05	0.12	1
2166-10	54	0.97	0.02	0.01	1
2166-11	24	0.61	0.31	0.08	1
2166-18	43	0.89	0.08	0.03	1
2166-24	36	0.92	0.05	0.03	1
2166-25	38	0.62	0.38	0.01	1
2166-3	30	0.81	0.1	0.09	1
2166-8	47	0.79	0.17	0.04	1
2166-9	45	0.93	0.03		1
Shp-2	37	0.89	0.1	0.01	1
8520/11	104	0.89	0.1	0.01	2
8520/40	41	0.98	0.02	0	2
502b-105	56	0.95	0.04	0.01	2
8530/14	16	0.72	0.21	0.07	2
652a*	108	0.94	0.05	0.01	2
647*	145	0.87	0.13	0.01	2
SHC*	115	0.77	0.22	0.01	2
878-01	104	0.96	0.04	0.01	2
210-y/76	190	0.89	0.1	0.01	2
SHCst	124	0.86	0.13	0.01	2
Vt4	75	0.78	0.2	0.02	2
Vt5	85	0.83	0.17	0	2
Vt7	90	0.85	0.15	0	2
Vt8	152	0.97	0.03	0	2
Vt11	157	0.86	0.14	0	2
Vt12	187	0.87	0.13	0	2
Vt15	35	0.58	0.41	0.01	2
IA1	6	0.32	0.08	0.6	2
IA2	34	0.97	0.03	0	2
IA3	31	0.81	0.18	0.01	2
IA2a	58	0.9	0	0.1	2
IA675	13	0.93	0.01	0.06	2
Y-1	62	0.82	0.16	0.02	2
Y-2	80	0.99	0.01	0	2
Y-4	63	0.97	0.02	0.01	2
IA-388	98	0.87	0.12	0.01	2

Reference: (1) Goncharov et al., 2015, (2) this study. $\text{H}_2\text{O}^{\text{xen}} = (\sum_{i=1}^n (\text{H}_2\text{O}_{\text{miner}}^{\text{mineral}}) \times \text{mod\%}_{\text{miner}}^{\text{mineral}})$, where $\text{H}_2\text{O}_{\text{miner}} = (\text{OH}^- + \text{H}_2\text{O}_{\text{cryst}})$, calculated for each mineral with its modal content ($\text{mod\%}_{\text{miner}}$).

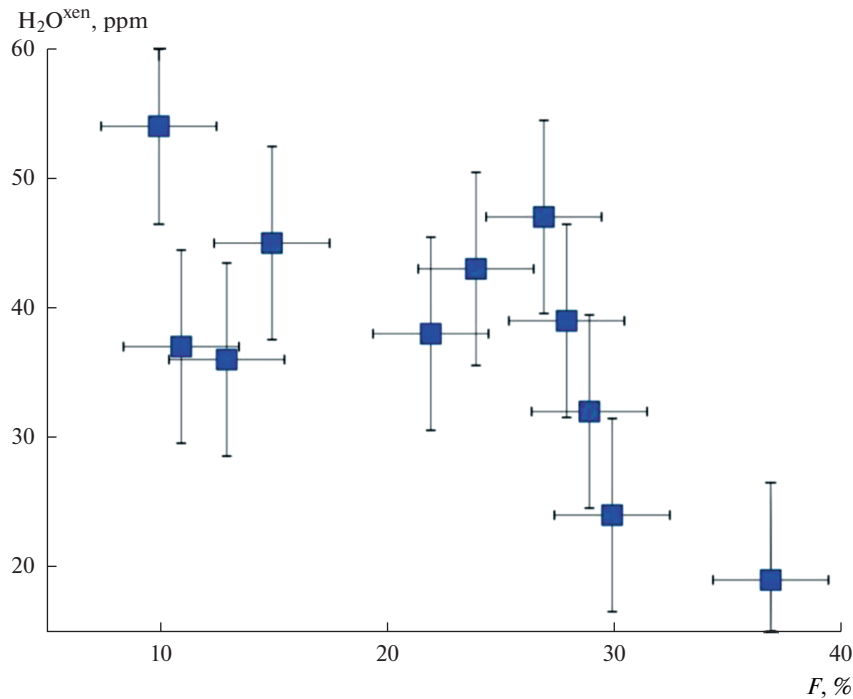


Fig. 11. Dependence of total water content ($\text{H}_2\text{O}^{\text{xen}}$) in Spitsbergen peridotite xenoliths vs the partial melting degree (F).

Рис. 11. Зависимость содержания воды ($\text{H}_2\text{O}^{\text{xen}}$) в ксенолитах Шпицбергена от степени парциального плавления (F).

$$F(\% \pm 5\%) = -276 + 355.4(\text{Mg/Si}) - 93.4(\text{Mg/Si})^2. \quad (2)$$

Negative dependence of the water content in peridotites on the degree of partial melting of peridotite is clearly visible (Fig. 11). Decrease of the water content in xenoliths with increase of partial melting degree allows us to suggest that the main mechanism of releasing of water is the partial melting of mantle rocks.

CONCLUSIONS

The novelty of this work lies in the application of two independent methods (FTIR and STA + QMS) to determine the volatile content in the crystal structure of exact the same samples of natural mantle minerals. This approach shows the presence of hydrogen in the forms of OH⁻ ions and molecules of crystal hydrate water ($\text{H}_2\text{O}_{\text{cryst}}$), as well as formations of carbon, including C—O and C—H bonds, such as CO₂, CH, CH₂, CH₃ groups in crystal structures. Water (total of OH⁻ and H₂O_{cryst}) is predominant among other studied C—O—H bonds according to these methods.

The obtained data indicate that lithospheric mantle rocks are potential source of C—O—H fluids itself, as there are various forms of hydrogen and carbon in the crystal structures of rock-forming minerals of peridotites and pyroxenites in a wide range of temperature (from 750 to 1450 °C), pressure (from 1.5 to 5.5 GPa) and the oxygen fugacity (from -4.5 to $+0.3 \log$

units relative to FMQ buffer). Major mechanism of release of these volatiles from the minerals is, probably, partial melting process.

We thank E.A. Vasiliev (Mining University, Saint Petersburg), D.A. Medvedeva (Institute of Macromolecular Compound RAS, Saint Petersburg), and A. Karaman for assistance with manuscript preparation. The research was supported by RSF (project No. 17-77-10103) and RFBR (project No. 10-05-01017, 11-05-00346). The work was carried out within the framework of the state budget theme of the IGGD RAS (No. 0153-2015-0006).

REFERENCES

- Ardia P., Hirschmann M.M., Withers A.C., Tenner T.J.* H₂O storage capacity of olivine at 5–8 GPa and consequences for dehydration partial melting of the upper mantle. *Earth Planet. Sci. Lett.* **2012**. Vol. 345–348. P. 104–116.
- Babushkina M.S., Nikitina L.P., Goncharov A.G., Ponomareva N.I.* Water in the structure of minerals from mantle peridotites as controlled by thermal and redox conditions in the upper mantle. *Geol. Ore Deposits.* **2009**. Vol. 51. P. 712–722.
- Babushkina M.S., Ugolkov V.L., Marin Yu.B., Nikitina L.P., Goncharov A.G.* Hydrogen and carbon groups in the structures of rock-forming minerals of rocks of the lithospheric mantle: FTIR and STA + QMS data. *Doklady Earth Sci.* **2018**. Vol. 479. P. 456–459.
- Bai Q., Kohlstedt D.L.* Substantial hydrogen solubility in olivine and implications for water storage in the mantle. *Nature.* **1992**. Vol. 357. P. 672–674.
- Balan E., Blanchard M., Lazzeri M., Ingrin J.* Contribution of interstitial OH groups to the incorporation of water in forsterite. *Phys. Chem. Miner.* **2014**. Vol. 41. P. 105–114.
- Bali E., Bolfan-Casanova N., Koga K.T.* Pressure and temperature dependence of H solubility in forsterite: An implication to water activity in the Earth interior. *Earth Planet. Sci. Lett.* **2008**. Vol. 268. P. 354–363.
- Bell D.R., Rossman G.R.* The distribution of hydroxyl in garnets from the subcontinental mantle of southern Africa. *Contrib. Miner. Petrol.* **1992a**. Vol. 111. P. 161–178.
- Bell D.R., Rossman G.R.* Water in Earth's mantle: The role of nominally anhydrous minerals. *Science.* **1992**. Vol. 255. P. 1391–1396.
- Bell D.R., Ihinger P.D., Rossman G.R.* Quantitative analysis of trace OH in garnet and pyroxenes. *Amer. Miner.* **1995**. Vol. 80 P. 465–474.
- Bell D.R., Rossman G.R., Maldener J., Endisch D., Rauch F.* Hydroxide in olivine: A quantitative determination of the absolute amount and calibration of the IR spectrum. *J. Geophys. Res. B: Solid Earth.* **2003**. Vol. 108. ECV 8-1-8-9.
- Berry A.J., O'Neill H.S.C., Hermann J., Scott D.R.* The infrared signature of water associated with trivalent cations in olivine. *Earth Planet. Sci. Lett.* **2007**. Vol. 261. P. 134–142.
- Demouchy S., Bolfan-Casanova N.* Distribution and transport of hydrogen in the lithospheric mantle: A review. *Lithos.* **2016**. Vol. 240–243. P. 402–425.
- Doucet L.S., Peslier A.H., Ionov D.A., Brandon A.D., Golovin A. V., Goncharov A.G., Ashchepkov I.V.* High water contents in the Siberian cratonic mantle linked to metasomatism: An FTIR study of Udachnaya peridotite xenoliths. *Geochim. Cosmochim. Acta.* **2014**. Vol. 137. P. 159–187.
- Férot A., Bolfan-Casanova N.* Water storage capacity in olivine and pyroxene to 14 GPa: Implications for the water content of the Earth's upper mantle and nature of seismic discontinuities. *Earth Planet. Sci. Lett.* **2012**. Vol. 349–350. P. 218–230.
- Freund F.* Mechanism of the water and carbon dioxide solubility in oxides and silicates and the role of O. *Contrib. Miner. Petrol.* **1981**. Vol. 76 P. 474–482.
- Freund F., Tsong I.S.T., Knipping U.* Solute carbon and carbon segregation in magnesium oxide single crystals – a secondary ion mass spectrometry study. *Phys. Chem. Miner.* **1986**. Vol. 13. P. 277–279.
- Freund F.T., Freund M.M.* From where did the water come that filled the Earth's oceans? A widely overlooked redox reaction. *Amer. J. Anal. Chem.* **2015**. Vol. 6. P. 342–349.
- Freund M.M., Freund F.T.* Solid solution model for interstellar dust grains and their organics. *Astrophys. J.* **2006**. Vol. 639. P. 210–226.
- Gavrilenko P.* Water solubility in diopside. Bayreuth: Universität Bayreuth, **2008**. 144 pp.
- Geiger C.A., Langer K., Bell D.R., Rossman G.R., Winkler B.* The hydroxide component in synthetic pyrope. *Amer. Miner.* **1991**. Vol. 76. P. 49–59.
- Glebovitsky V.A., Nikitina L.P., Saltykova A.K., Pushkarev Y.D., Ovchinnikov N.O., Babushkina M.S., Ashchepkov I.V.* Thermal and chemical heterogeneity of the upper mantle beneath the Baikal-Mongolia territory. *Petrology.* **2007**. Vol. 15. P. 58–89.

- Goncharov A.G., Ionov D.A. Redox state of deep off-craton lithospheric mantle: New data from garnet and spinel peridotites from Vitim, southern Siberia. *Contrib. Miner. Petrol.* **2012**. Vol. 164. P. 731–745.
- Goncharov A.G., Ionov D.A., Doucet L.S., Pokhilenko L.N. Thermal state, oxygen fugacity and C–O–H fluid speciation in cratonic lithospheric mantle: New data on peridotite xenoliths from the Udachnaya kimberlite, Siberia. *Earth Planet. Sci. Lett.* **2012**. 357–358. P. 99–110.
- Goncharov A.G., Nikitina L.P., Borovkov N.V., Babushkina M.S., Sirokin A.N. Thermal and redox equilibrium conditions of the upper-mantle xenoliths from the Quaternary volcanoes of NW Spitsbergen, Svalbard Archipelago. *Russian Geol. Geophys.* **2015**. Vol. 56. P. 1578–1602.
- Grant K., Ingrin J., Lorand J., Dumas P. Water partitioning between mantle minerals from peridotite xenoliths. *Contrib. Miner. Petrol.* **2007**. Vol. 154. P. 15–34.
- Gudmundsson G., Wood B.J. Experimental tests of garnet-peridotite oxygen barometry. *Contrib. Miner. Petrol.* **1995**. Vol. 119. P. 56–67.
- Ingrin J., Latrous K., Doukhan J.C., Doukhan N. Water in diopside: an electron microscopy and infrared spectroscopy study. *Europ. J. Miner.* **1989**. Vol. 1. P. 327–341.
- Jacobsen S.D., Demouchy S., Frost D.J., Ballaran T.B., Kung, J. A systematic study of OH in hydrous wadsleyite from polarized FTIR spectroscopy and single-crystal X-ray diffraction: Oxygen sites for hydrogen storage in Earth's interior. *Amer. Miner.* **2005**. Vol. 90. P. 61–70.
- Kadik A.A. Oxygen fugacity regime in the upper mantle as a reflection of the chemical differentiation of planetary materials. *Geochem. Int.* **2006**. Vol. 44. P. 56–71.
- Karato S.I. Remote sensing of hydrogen in Earth's mantle. *Rev. Miner. Geochem.* **2006**. Vol 62. P. 343–375.
- Khisina N.R., Wirth R., Andrut M., Ukhakov A.V. Extrinsic and intrinsic mode of hydrogen occurrence in natural olivines: FTIR and TEM investigation. *Phys. Chem. Miner.* **2001**. Vol. 28. P. 291–301.
- Khisina N.R., Wirth R. Hydrous olivine in mantle olivine. *Phys. Chem. Miner.* **2002**. Vol. 29. P. 98–111.
- Khisina N., Wirth R., Matsyuk S., Koch-Müller M. Microstructures and OH-bearing nano-inclusions in “wet” olivine xenocrysts from the Udachnaya kimberlite. *Europ. J. Miner.* **2008**. Vol. 20. P. 1067–1078.
- Koch-Müller M., Matsyuk S.S., Wirth R. Hydroxyl in omphacites and omphacitic clinopyroxenes of upper mantle to lower crustal origin beneath the Siberian platform. *Amer. Miner.* **2004**. Vol. 89. P. 921–931.
- Koch-Müller M., Matsyuk S.S., Rhede D., Wirth R., Khisina N. Hydroxyl in mantle olivine xenocrysts from the Udachnaya kimberlite pipe. *Phys. Chem. Miner.* **2006**. Vol. 33. P. 276–287.
- Koch-Müller M., Abs-Wurmbach I., Rhede D., Kahlenberg V., Matsyuk, S. Dehydration experiments on natural omphacites: Qualitative and quantitative characterization by various spectroscopic methods. *Phys. Chem. Miner.* **2007**. Vol. 34. P. 663–678.
- Kohlstedt D.L., Keppler H., Rubie D.C. Solubility of water in the α , β and γ phases of $(\text{Mg}, \text{Fe})_2\text{SiO}_4$. *Contrib. Miner. Petrol.* **1996**. Vol. 123. P. 345–357.
- Kohn S.C., Brooker R.A., Frost D.J., Slesinger A.E., Wood B.J. Ordering of hydroxyl defects in hydrous wadsleyite (β - Mg_2SiO_4). *Amer. Miner.* **2002**. Vol. 87. P. 293–301.
- Kovács I., Hermann J., O'Neill H.S.C., Gerald J.F., Cambridge M., Horváth G. Quantitative absorbance spectroscopy with unpolarized light: Part II. Experimental evaluation and development of a protocol for quantitative analysis of mineral IR spectra. *Amer. Miner.* **2008**. Vol. 93. P. 765–778.
- Lazarev A.N. Vibrational Spectra and Structure of Silicates. New York: Springer, **1995**. 302 p.
- Litasov K.D., Shatskiy A.F., Pal'yanov Y.N., Sokol A.G., Katsura T., Ohtani, E. Hydrogen incorporation into forsterite in Mg_2SiO_4 – $\text{K}_2\text{Mg}(\text{CO}_3)_2$ – H_2O and Mg_2SiO_4 – H_2O –C at 7.5–14.0 GPa. *Russian Geol. Geophys.* **2009**. Vol. 50. P. 1129–1138.
- Liu J., Xia Q.K., Deloule E., Ingrin J., Chen H., Feng M. Water content and oxygen isotopic composition of alkali basalts from the Taihang Mountains, China: recycled oceanic components in the mantle source. *J. Petrol.* **2015**. Vol. 56. P. 681–702.
- Mathez E.A., Blacic J.D., Beery J., Maggiore C., Hollander M. Carbon abundances in mantle minerals determined by nuclear reaction analysis. *Geophys. Res. Lett.* **1984**. Vol. 11. P. 947–950.
- Matsyuk S.S., Langer K. Hydroxyl in olivines from mantle xenoliths in kimberlites of the Siberian platform. *Contrib. Miner. Petrol.* **2004**. Vol. 147. P. 413–437.
- Matsyuk S.S., Langer K., Hösch A. Hydroxyl defects in garnets from mantle xenoliths in kimberlites of the Siberian platform. *Contrib. Miner. Petrol.* **1998**. Vol. 132. P. 163–179.
- Mierdel K., Keppler H., Smyth J.R., Langenhorst F. Water solubility in aluminous orthopyroxene and the origin of earth's asthenosphere. *Science.* **2007**. Vol. 315. P. 364–368.
- Mosenfelder J.L., Rossman G.R. Analysis of hydrogen and fluorine in pyroxenes: I. Orthopyroxene. *Amer. Miner.* **2013a**. Vol. 98. P. 1026–1041.
- Mosenfelder J.L., Rossman G.R. Analysis of hydrogen and fluorine in pyroxenes: II. Clinopyroxene. *Amer. Mineral.* **2013b**. Vol. 98. P. 1042–1054.

- Mosenfelder J.L., Deligne N.I., Asimow P.D., Rossman G.R. Hydrogen incorporation in olivine from 2–12 GPa. *Amer. Miner.* **2006**. Vol. 91. P. 285–294.
- Murakami M., Hirose K., Yurimoto H., Nakashima S., Takafuji N. Water in earth's lower mantle. *Science*. **2002**. Vol. 295. P. 1885–1887.
- Nikitina L.P., Goncharov A.G., Saltykova A.K., Babushkina M.S. The redox state of the continental lithospheric mantle of the Baikal-Mongolia region. *Geochem. Int.* **2010**. Vol. 48. P. 15–40.
- Nikitina L.P., Bogomolov E.S., Krymsky R.S., Belyatsky B. V., Korolev N.M., Zinchenko V.N. Nd–Sr–Os systems of eclogites in the lithospheric mantle of the Kasai Craton (Angola). *Russian Geol. Geophys.* **2017**. Vol. 58. P. 1305–1316.
- Ponomarev B.G., Lapides I.L. Hydroxyl probe in micas: analysis of the distribution of cations in the tetrahedra and octahedra from IR spectra. In: *Abstr. Sixth All-Union Symp. Isomorphism*. Zvenigorod, **1988**. P. 175 (in Russian).
- Ponomarev B.G., Lapides I.L. IR spectra of hydroxyl in layered silicates: vacancies in biotite. *Miner. J.* **1990**. P. 78–82 (in Russian).
- Rauch M., Keppler H. Water solubility in orthopyroxene. *Contrib. Miner. Petrol.* **2002**. Vol. 143. P. 525–536.
- Rousseaux J.M., Gomez Laverde C., Nathan Y., Rouxhet P.G. Correlation between the hydroxyl stretching bands and the chemical composition of trioctahedral micas. In: *Proc. Inter. Clay Conf. Madrid. Division de Ciencias CSIC*. Madrid, **1972**. P. 89–98.
- Sambridge M., Gerald J.F., Kovács I., O'Neill H.S.C., Hermann J. Quantitative absorbance spectroscopy with unpolarized light: Part I. Physical and mathematical development. *Amer. Miner.* **2008**. Vol. 93. N. 5–6. P. 751–764.
- Shcheka S.S., Wiedenbeck M., Frost D.J., Keppler H. Carbon solubility in mantle minerals. *Earth Planet. Sci. Lett.* **2006**. Vol. 245. P. 730–742.
- Skogby H., Bell D.R., Rossman G.R. Hydroxide in pyroxene: variations in the natural environment. *Amer. Miner.* **1990**. Vol. 75. P. 764–774.
- Smyth J.R., Kawamoto T., Jacobsen S.D., Swope R.J., Hervig R.L., Holloway J.R. Crystal structure of monoclinic hydrous wadsleyite $[\beta\text{-}(\text{Mg}, \text{Fe})_2\text{SiO}_4]$. *Amer. Miner.* **1997**. Vol. 82. P. 270–275.
- Smyth J.R., Mierdel K., Keppler H., Langenhorst F., Dubrovinsky L., Nestola F. Crystal chemistry of hydration in aluminous orthopyroxene. *Amer. Miner.* **2007**. Vol. 92. P. 973–976.
- Stalder R. Influence of Fe, Cr and Al on hydrogen incorporation in orthopyroxene. *Europ. J. Miner.* **2004**. Vol. 16. P. 703–711.
- Stalder R., Ludwig T. OH incorporation in synthetic diopside. *Europ. J. Miner.* **2007**. Vol. 19. P. 373–380.
- Tingle T.N., Green H.W. Carbon solubility in olivine: Implications for upper mantle evolution *Geology*. **1987**. Vol. 15. P. 324–326.
- Tingle T.N., Green H.W., Finnerty A.A. Experiments and observations bearing on the solubility and diffusivity of carbon in olivine. *J. Geophys. Res.* **1988**. Vol. 93. P. 215–289, 304.
- Tsong I.S.T., Knipping U., Loxton C.M., Magee C.W., Arnold G.W. Carbon on surfaces of magnesium oxide and olivine single crystals. Diffusion from the bulk or surface contamination? *Phys. Chem. Miner.* **1985**. Vol. 12. P. 261–270.
- Withers A.C., Hirschmann M.M. H_2O storage capacity of MgSiO_3 clinoenstatite at 8–13 GPa, 1,100–1,400 °C. *Contrib. Miner. Petrol.* **2007**. Vol. 154. P. 663–674.
- Withers A.C., Hirschmann M.M. Influence of temperature, composition, silica activity and oxygen fugacity on the H_2O storage capacity of olivine at 8 GPa. *Contrib. Miner. Petrol.* **2008**. Vol. 156. P. 595–605.
- Wood B.J. Oxygen barometry of spinel peridotites. *Rev. Miner.* **1991**. Vol. 25. P. 417–431.
- Xia Q. K., Liu J., Liu S. C., Kovács I., Feng M., Dang L. High water content in Mesozoic primitive basalts of the North China Craton and implications on the destruction of cratonic mantle lithosphere. *Earth Planet. Sci. Lett.* **2013**. Vol. 361. P. 85–97.
- Yang X.-Z.Z., Xia Q.-K.K., Deloule E., Dallai L., Fan Q.-C.C., Feng M. Water in minerals of the continental lithospheric mantle and overlying lower crust: A comparative study of peridotite and granulite xenoliths from the North China Craton. *Chem. Geol.* **2008**. Vol. 256. P. 33–45.
- Yang X. OH solubility in olivine in the peridotite–COH system under reducing conditions and implications for water storage and hydrous melting in the reducing upper mantle. *Earth Planet. Sci. Lett.* **2015**. Vol. 432. P. 199–209.

**ФОРМЫ ВОДЫ И УГЛЕРОДА В СТРУКТУРЕ НОМИНАЛЬНО БЕЗВОДНЫХ
МИНЕРАЛОВ ПОРОД ЛИТОСФЕРНОЙ МАНТИИ:
КОМПЛЕКСНОЕ ФУРЬЕ-ИК-СПЕКТРОСКОПИЧЕСКОЕ
И STA + QMS ИССЛЕДОВАНИЕ**

Д. чл. М. С. Бабушкина^{a, *}, д. чл. Л. П. Никитина^a, А. Г. Гончаров^{a, b}, В. Л. Уголков^c

^aИнститут геологии и геохронологии докембра РАН,
наб. Макарова, 2, Санкт-Петербург, 199034 Россия

^bСанкт-Петербургский государственный университет, Институт наук о Земле,
Университетская наб., 7/9, Санкт-Петербург, 199034 Россия

^cИнститут химии силикатов РАН, наб. Макарова, 2, Санкт-Петербург, 199034 Россия

*e-mail: msbab@mail.ru

Присутствие водорода в форме ионов OH^- , молекул кристаллогидратной воды $\text{H}_2\text{O}_{\text{cryst}}$ и углерода в виде CH , CH_2 , CH_3 и CO_2 в кристаллической структуре минералов из мантийных перidotитов и пироксенитов установлено методом Фурье-ИК-спектроскопии и подтверждено комплексным термическим анализом в сочетании с квадрупольной масс-спектроскопией продуктов разложения (STA + QMS). Температура выделения $m17$ (OH^-) (данные STA + QMS) выше по сравнению с $m18$ ($\text{H}_2\text{O}_{\text{cryst}}$), что свидетельствует о более слабых связях $\text{H}_2\text{O}_{\text{cryst}}$ с кристаллической структурой и подтверждается более высокими волновыми числами v_{OH^-} (данные Фурье-ИК-спектроскопии) по сравнению с $v_{\text{H}_2\text{O}_{\text{cryst}}}$. Суммарное содержание воды $\text{H}_2\text{O}^{\text{miner}} = (\text{OH}^- + \text{H}_2\text{O}_{\text{cryst}})$, являющейся преобладающим компонентом среди летучих, составляет (ppm): 10–230 в форстерите, 40–400 в диопside, 20–220 в энстатите, 30–340 в пиропе. Содержание воды в ксенолитах варьирует от 20 до 200 ppm. Летучие в структуре минералов сохраняются при температуре 750–1450 °C, давлении 1.5–5.5 ГПа и фугитивности кислорода $\Delta g_{\text{O}_2}^{\text{FMQ}} -4.5...+0.3$, а основным механизмом их выделения является, вероятно, процесс частичного плавления породы: общее содержание водной составляющей уменьшается с увеличением его степени.

Ключевые слова: водород, углерод, Фурье-ИК-спектроскопия, комплексный термический анализ (STA) и квадрупольная масс-спектрометрия (QMS), ксенолиты литосферной мантии, перidotиты, пироксениты, номинально безводные минералы